Acta Mech 224, 1335–1349 (2013)
DOI 10.1007/s00707-013-0811-8

J. G. Yu · J. E. Lefebvre · Y. Q. Guo

Wave propagation in multilayered piezoelectric spherical plates

Received: 24 September 2012 / Revised: 17 December 2012 / Published online: 26 January 2013

Abstract This paper proposes an improvement of the Legendre polynomial series method to solve the harmonic wave propagation in multilayered piezoelectric spherical plates, which are used in point-focusing transducers. The conventional Legendre polynomial method can deal with the multilayered structures only when the material properties of two adjacent layers do not change significantly and cannot obtain correctly normal stress and normal electric displacement shapes unlike the proposed improved orthogonal polynomial approach which overcomes these drawbacks. Detailed formulations are given to highlight its differences from the conventional Legendre polynomial approach. Through the comparisons of numerical results given by an exact solution (obtained from the reverberation-ray matrix method), and by the conventional polynomial approach and the improved polynomial approach, the validity of the proposed approach is illustrated. The influences of the radius-to-thickness ratio on dispersion curves, stress and electric displacement distributions are discussed. It is found that three factors determine the distribution of mechanical energy and electric energy at higher frequencies: radius-to-thickness ratio, wave speed, and position of the component material.

1 Introduction

Piezoelectric materials (PEM) allow to fabricate acoustic devices that are widely used in the fields of electrical engineering, mechanical engineering, and communications. To enhance piezoelectric materials' potentialities,

J. G. Yu (✉)
School of Mechanical and Power Engineering, Henan Polytechnic University,
Jiaozuo 454003, People's Republic of China
E-mail: yu@emails.bjut.edu.cn

J. E. Lefebvre
University Lille Nord de France, 59000 Lille, France

Y. Q. Guo
Key Laboratory of Mechanics on Disaster and Environment in Western China,
Ministry of Education, Lanzhou, People's Republic of China

Y. Q. Guo
School of Civil Engineering and Mechanics, Lanzhou University,
Lanzhou 730000, People's Republic of China

J. E. Lefebvre
UVHC, IEMN-DOAE, 59313 Valenciennes Cedex 9, France

J. E. Lefebvre
CNRS, UMR 8520, 59650 Villeneuve d'Ascq, France

piezoelectric structures are often designed in the form of multilayered structures to meet specific application purposes.

For design and optimization purposes, appropriate theoretical models and efficient numerical methods are highly desirable to investigate wave propagation behavior in layered piezoelectric structures. There have been numerous methods to model this problem, such as the finite element method [1,2], the transfer matrix method [3–5], the reverberation-ray matrix method [6], the layer element method [7,8], the scattering matrix method [9], the orthogonal polynomial series method [10,11], and so on. Among various geometries, layered piezoelectric flat plates and hollow cylinders have all attracted considerable attention. But the layered piezoelectric spherical plates, which are used in point-focusing transducers, received very limited attentions.

This paper proposes an improved orthogonal polynomial series method to investigate the harmonic wave propagation in multilayered spherical curved plates. The improved method overcomes the limitations of the conventional orthogonal polynomial method, which has been used to solve the wave motion for about forty years, from Laguerre polynomial for half infinite media [12,13] to Legendre polynomial for finite thickness structures [14,15], from homogeneous structures [16] to multilayered structures [10,17] and to functionally graded structures [18,19], from pure elastic structures [20] to various multi-field coupled structures [21–23], from a flat plate [11] to various curved structures [24–26]. All these references show that the orthogonal polynomial series method is quite versatile to calculate wave motion in quite various structures.

However, the orthogonal polynomial series method can deal with the layered plates only when the material properties of two adjacent layers do not change significantly and cannot obtain correct continuous normal stress and normal electric displacement profiles. The conventional orthogonal polynomial method uses a single polynomial expansion which is continuous in level and in slope over the entire structure even at the frontier between two adjacent layers. This results in continuous mechanical displacement and electric potential distributions in level and in slope and therefore discontinuous normal stress and normal electric displacement distributions because of different material constants of two adjacent layers. But for such a real structure, the true or physical mechanical displacement and electric potential are continuous at the interfaces between two adjacent layers, but their derivatives are not. These discontinuous derivatives with different elastic constants allow the normal stress and normal electric displacement components to be continuous.

In this paper, detailed formulations of the improved orthogonal polynomial method are given to highlight the differences to the conventional polynomial approach. The validity of the improved method is verified by numerical comparisons. The influences of the radius-to-thickness ratio and the stacking sequence on dispersion curves, stress and electric displacement distributions are discussed.

2 Mathematics and formulation of the problem

Consider an orthotropic N-layered piezoelectric spherical plate which is polarized in radial direction with a total thickness h, as shown in Fig. 1. In the spherical coordinate system (θ, φ, r), a and b are the inner and outer radii. The outer radius-to-thickness ratio is defined as $\eta = b/h$.

For the wave propagation considered in this paper, the body forces and electric charges are assumed to be zero. Thus, the dynamic equation for the layered piezoelectric spherical plate is governed by

$$\begin{aligned}
\frac{\partial T_{rr}}{\partial r} + \frac{1}{r}\frac{\partial T_{r\theta}}{\partial \theta} + \frac{1}{r\sin\theta}\frac{\partial T_{r\phi}}{\partial \phi} + \frac{2T_{rr} + T_{r\theta}\cot\theta - T_{\theta\theta} - T_{\phi\phi}}{r} &= \rho\frac{\partial^2 u_r}{\partial t^2},\\
\frac{\partial T_{r\theta}}{\partial r} + \frac{1}{r}\frac{\partial T_{\theta\theta}}{\partial \theta} + \frac{1}{r\sin\theta}\frac{\partial T_{\theta\phi}}{\partial \phi} + \frac{3T_{r\theta} + \cot\theta\left(T_{\theta\theta} - T_{\phi\phi}\right)}{r} &= \rho\frac{\partial^2 u_\theta}{\partial t^2},\\
\frac{\partial T_{r\phi}}{\partial r} + \frac{1}{r}\frac{\partial T_{\theta\phi}}{\partial \theta} + \frac{1}{r\sin\theta}\frac{\partial T_{\phi\phi}}{\partial \phi} + \frac{3T_{r\phi} + 2T_{\theta\phi}\cot\theta}{r} &= \rho\frac{\partial^2 u_z}{\partial t^2},\\
\frac{\partial D_r}{\partial r} + \frac{1}{r}\frac{\partial D_\theta}{\partial \theta} + \frac{1}{r\sin\theta}\frac{\partial D_\phi}{\partial \phi} + \frac{2D_r + D_\theta\cot\theta}{r} &= 0
\end{aligned} \tag{1}$$

where T_{ij}, u_i, and D_i are the stress, mechanical displacements, and electric displacements, respectively; ρ is the density of the material.

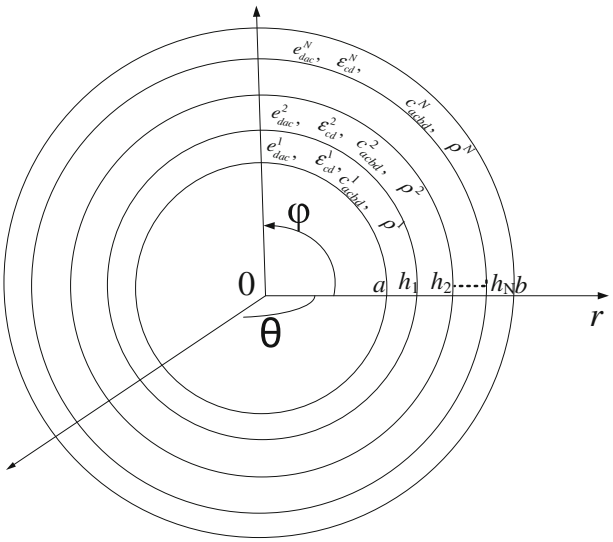

Fig. 1 Schematic diagram of a multilayered piezoelectric spherical plate

The relationships between the general strain and general displacement can be expressed as

$$\begin{aligned}
&\varepsilon_{\theta\theta} = \frac{1}{r}\frac{\partial u_\theta}{\partial\theta} + \frac{u_r}{r},\ \varepsilon_{\phi\phi} = \frac{1}{r\sin\theta}\frac{\partial u_\phi}{\partial\phi} + \frac{u_r}{r} + \frac{\cot\theta}{r}u_\theta,\ \varepsilon_{rr} = \frac{\partial u_r}{\partial r},\\
&\varepsilon_{r\theta} = \frac{1}{2}\left(\frac{1}{r}\frac{\partial u_r}{\partial\theta} + \frac{\partial u_\theta}{\partial r} - \frac{u_\theta}{r}\right),\ \varepsilon_{r\phi} = \frac{1}{2r}\left(\frac{1}{\sin\theta}\frac{\partial u_r}{\partial\phi} - u_\phi\right) + \frac{1}{2}\frac{\partial u_\phi}{\partial r},\\
&\varepsilon_{\theta\phi} = \frac{1}{2r}\left(\frac{1}{\sin\theta}\frac{\partial u_\theta}{\partial\phi} + \frac{\partial u_\phi}{\partial\theta} - u_\phi\cot\theta\right),\ E_\theta = -\frac{1}{r}\frac{\partial\Phi}{\partial\theta},\ E_\phi = -\frac{1}{r\sin\theta}\frac{\partial\Phi}{\partial\phi},\ E_r = -\frac{\partial\Phi}{\partial r},
\end{aligned} \tag{2}$$

where ε_{ij}, E_i, and Φ are the strain, the electric field, and the electric potential, respectively.

The traction-free and open circuit boundary conditions for a multilayered piezoelectric structure require that (i) the mechanical displacement, the normal components of the stress, and the electric displacement should be continuous at the interfaces; (ii) the normal components of the stress and of the electric displacement should be zero at the inner and outer surfaces.

By introducing the rectangular window function $\pi_{a,h_N}(r)$

$$\pi_{a,h_N}(r) = \begin{cases} 1, & a \le r \le h_N \\ 0, & \text{elsewhere} \end{cases},$$

the traction-free and open circuit boundary conditions ($T_{rr} = T_{r\theta} = T_{r\varphi} = 0$ and $D_r = 0$ at $r = h_0 = a$ and $r = h_N = b$) are automatically incorporated in the constitutive relations of the plate [10]:

$$\begin{aligned}
T_{\theta\theta} &= C_{11}\varepsilon_{\theta\theta} + C_{12}\varepsilon_{\varphi\varphi} + C_{13}\varepsilon_{rr} - e_{31}E_r,\\
T_{\varphi\varphi} &= C_{12}\varepsilon_{\theta\theta} + C_{22}\varepsilon_{\varphi\varphi} + C_{23}\varepsilon_{rr} - e_{32}E_r,\\
T_{rr} &= (C_{13}\varepsilon_{\theta\theta} + C_{23}\varepsilon_{\varphi\varphi} + C_{33}\varepsilon_{rr} - e_{33}E_r)\pi_{a,h_N}(r),\\
T_{r\varphi} &= \left(2C_{44}\varepsilon_{r\varphi} - e_{24}E_\varphi\right)\pi_{a,h_N}(r),\\
T_{r\theta} &= (2C_{55}\varepsilon_{r\theta} - e_{15}E_\theta)\,\pi_{a,h_N}(r),\\
T_{\theta\varphi} &= 2C_{66}\varepsilon_{\theta\varphi},
\end{aligned} \tag{3.1}$$

$$\begin{aligned}
D_\theta &= 2e_{15}\varepsilon_{r\theta} + \in_{11} E_\theta,\\
D_\varphi &= 2e_{24}\varepsilon_{r\varphi} + \in_{22} E_\varphi,\\
D_r &= \left(e_{31}\varepsilon_{\theta\theta} + e_{32}\varepsilon_{\varphi\varphi} + e_{33}\varepsilon_{rr} + \in_{33} E_r\right)\pi_{a,h_N}(r)
\end{aligned} \tag{3.2}$$

where C_{ij}, e_{ij}, and $\in_{ij}$ are, respectively, the elastic, piezoelectric, and dielectric coefficients given in the crystallographic axes.

The elastic coefficients of the layered spherical plate are expressed as

$$C_{ij} = \sum_{n=1}^{N} C_{ij}^{n} \pi_{h_{n-1},h_n}(r), \tag{4.1}$$

where N is the number of the layers and C_{ij}^{n} are the elastic constants of the Nth material. Similarly, the other material coefficients can be expressed as

$$e_{ij} = \sum_{n=1}^{N} e_{ij}^{n} \pi_{h_{n-1},\, h_n}(r),\ \in_{ij} = \sum_{n=1}^{N} \in_{ij}^{n} \pi_{h_{n-1},h_n}(r),\ \rho = \sum_{n=1}^{N} \rho^{n} \pi_{h_{n-1},h_n}(r). \tag{4.2}$$

According to Kargl and Marston [27] and Towfighi and Kundu [28], the wave front on the surface of a spherical shell is assumed to be toroidal. In addition, to study wave propagation in a spherical plate segment from point A to B, the two points A and B can always be aligned along the equator of a sphere by adjusting the positions of the north and south poles. Therefore, to study the wave propagation between two points in a spherical plate segment, it is sufficient to solve the governing equations for $\theta = \pi/2$ only. Thus, the propagating wave is independent of θ. Then, the displacement components of this toroidal wave can be written as

$$u_r(r,\theta,\varphi,t) = \exp(ikb\varphi - i\omega t)U(r), \tag{5.1}$$
$$u_\theta(r,\theta,\varphi,t) = \exp(ikb\varphi - i\omega t)V(r), \tag{5.2}$$
$$u_\varphi(r,\theta,\varphi,t) = \exp(ikb\varphi - i\omega t)W(r), \tag{5.3}$$
$$\Phi(x,y,\varphi,t) = \exp(ikb\varphi - i\omega t)X(r). \tag{5.4}$$

$U(r)$, $V(r)$, $W(r)$ represent the amplitude of vibration in the r, θ, φ directions and $X(r)$ represents the amplitude of the electric potential. k is the magnitude of the wave vector in the propagation direction, and ω is the angular frequency.

Substituting Eqs. (2), (3), (4), (5) into Eq. (1), the governing differential equations in terms of displacement and electric potential can be obtained:

$$\begin{aligned}
&\left(r^2U'' + 2rU'\right)\sum_{n=1}^{N} C_{33}^{n}\pi_{h_{n-1},h_n}(r) + \left(\sum_{n=1}^{N} C_{13}^{n}\pi_{h_{n-1},h_n}(r) + \sum_{n=1}^{N} C_{23}^{n}\pi_{h_{n-1},h_n}(r)\right)U \\
&-\left(\sum_{n=1}^{N} C_{11}^{n}\pi_{h_{n-1},h_n}(r) + \sum_{n=1}^{N} C_{22}^{n}\pi_{h_{n-1},h_n}(r) + 2\sum_{n=1}^{N} C_{12}^{n}\pi_{h_{n-1},h_n}(r)\right)U + (kb)^2 U\sum_{n=1}^{N} C_{44}^{n}\pi_{h_{n-1},h_n}(r) \\
&+ r^2U'\left(\sum_{n=1}^{N} C_{33}^{n}\pi_{h_{n-1},h_n}(r)\right)' + rU\left(\sum_{n=1}^{N} C_{13}^{n}\pi_{h_{n-1},h_n}(r)\right)' + rU\left(\sum_{n=1}^{N} C_{23}^{n}\pi_{h_{n-1},h_n}(r)\right)' \\
&+ ikb\left(rW' - W\right)\sum_{n=1}^{N} C_{44}^{n}\pi_{h_{n-1},h_n}(r) - ikb\left(\sum_{n=1}^{N} C_{11}^{n}\pi_{h_{n-1},h_n}(r) + \sum_{n=1}^{N} C_{22}^{n}\pi_{h_{n-1},h_n}(r)\right)W \\
&+ ikb\left(rW' + W\right)\sum_{n=1}^{N} C_{23}^{n}\pi_{h_{n-1},h_n}(r) + ikbrW\left(\sum_{n=1}^{N} C_{23}^{n}\pi_{h_{n-1},h_n}(r)\right)' \\
&+ \left(r^2X'' + 2rX'\right)\sum_{n=1}^{N} e_{33}^{n}\pi_{h_{n-1},h_n}(r) - \left(\sum_{n=1}^{N} e_{31}^{n}\pi_{h_{n-1},h_n}(r) + \sum_{n=1}^{N} e_{32}^{n}\pi_{h_{n-1},h_n}(r)\right)X' \\
&- (kb)^2 X\sum_{n=1}^{N} e_{24}^{n}\pi_{h_{n-1},h_n}(r) + r^2X'\left(\sum_{n=1}^{N} e_{33}^{n}\pi_{h_{n-1},h_n}(r)\right)' = -\omega^2 r^2 U\sum_{n=1}^{N} \rho^{n}\pi_{h_{n-1},h_n}(r),
\end{aligned} \tag{6.1}$$

$$
\begin{aligned}
&\left(r^2V''+2rV'\right)\sum_{n=1}^{N}C_{66}^{n}\pi_{h_{n-1},h_n}(r)\\
&-V\left[2\sum_{n=1}^{N}C_{66}^{n}\pi_{h_{n-1},h_n}(r)+\sum_{n=1}^{N}C_{23}^{n}\pi_{h_{n-1},h_n}(r)+(kb)^2\sum_{n=1}^{N}C_{44}^{n}\pi_{h_{n-1},h_n}(r)\right]\\
&+\left(r^2V'+rV\right)\left(\sum_{n=1}^{N}C_{66}^{n}\pi_{h_{n-1},h_n}(r)\right)'=-\omega^2r^2V\sum_{n=1}^{N}\rho^{n}\pi_{h_{n-1},h_n}(r), \qquad (6.2)\\
&\left(r^2W''+2rW'\right)\sum_{n=1}^{N}C_{44}^{n}\pi_{h_{n-1},h_n}(r)-\left(2\sum_{n=1}^{N}C_{44}^{n}\pi_{h_{n-1},h_n}(r)+(kb)^2\sum_{n=1}^{N}C_{22}^{n}\pi_{h_{n-1},h_n}(r)\right)W\\
&+\left(r^2W'-rW+ikbrU\right)\left(\sum_{n=1}^{N}C_{44}^{n}\pi_{h_{n-1},h_n}(r)\right)'+ikb\left(rU'+2U\right)\sum_{n=1}^{N}C_{44}^{n}\pi_{h_{n-1},h_n}(r)\\
&+W\sum_{n=1}^{N}C_{66}^{n}\pi_{h_{n-1},h_n}(r)+ikbU\left(\sum_{n=1}^{N}C_{12}^{n}\pi_{h_{n-1},h_n}(r)+\sum_{n=1}^{N}C_{22}^{n}\pi_{h_{n-1},h_n}(r)\right)+ikbrX'\sum_{n=1}^{N}e_{32}^{n}\pi_{h_{n-1},h_n}(r)\\
&+ikb\left(rX'+2X\right)\sum_{n=1}^{N}e_{24}^{n}\pi_{h_{n-1},h_n}(r)+ikbrX\left(\sum_{n=1}^{N}e_{24}^{n}\pi_{h_{n-1},h_n}(r)\right)'=-\omega^2r^2V\sum_{n=1}^{N}\rho^{n}\pi_{h_{n-1},h_n}(r), \qquad (6.3)\\
&\left(r^2U''+2rU'\right)\sum_{n=1}^{N}e_{33}^{n}\pi_{h_{n-1},h_n}(r)+\left(rU'+U\right)\left(\sum_{n=1}^{N}e_{31}^{n}\pi_{h_{n-1},h_n}(r)+\sum_{n=1}^{N}e_{32}^{n}\pi_{h_{n-1},h_n}(r)\right)\\
&-(kb)^2U\sum_{n=1}^{N}e_{24}^{n}\pi_{h_{n-1},h_n}(r)+rU\left(\sum_{n=1}^{N}e_{32}^{n}\pi_{h_{n-1},h_n}(r)\right)'+rU\left(\sum_{n=1}^{N}e_{31}^{n}\pi_{h_{n-1},h_n}(r)\right)'\\
&+r^2U'\left(\sum_{n=1}^{N}e_{33}^{n}\pi_{h_{n-1},h_n}(r)\right)'+ikb\left[\left(rW'+W\right)\sum_{n=1}^{N}e_{32}^{n}\pi_{h_{n-1},h_n}(r)+\left(rW'-W\right)\sum_{n=1}^{N}e_{24}^{n}\pi_{h_{n-1},h_n}(r)\right]\\
&+ikbrW\left(\sum_{n=1}^{N}e_{32}^{n}\pi_{h_{n-1},h_n}(r)\right)'-\left(r^2X''+2rX'\right)\sum_{n=1}^{N}\in_{33}^{n}\pi_{h_{n-1},h_n}(r)+(kb)^2X\sum_{n=1}^{N}\in_{22}^{n}\pi_{h_{n-1},h_n}(r)\\
&-r^2X'\left(\sum_{n=1}^{N}\in_{33}^{n}\pi_{h_{n-1},h_n}(r)\right)'=0 \qquad (6.4)
\end{aligned}
$$

where the superscript $(\,)'$ is the partial derivative with respect to r. Obviously, Eq. (6.2) is independent of the other three equations. It represents the propagating circumferential SH wave. The other two Eqs. (6.1) and (6.2) control the propagating circumferential Lamb-like waves and are coupled with Gauss' equation.

To solve the coupled wave Eq. (6), the conventional orthogonal polynomial approach expands $U(r)$, $V(r)$, $W(r)$, and $X(r)$ into four Legendre orthogonal polynomial series,

$$
U(r)=\sum_{m=0}^{\infty}p_m^1Q_m(r),\ V(r)=\sum_{m=0}^{\infty}p_m^2Q_m(r),\ \ W(r)=\sum_{m=0}^{\infty}p_m^3Q_m(r),\ \ X(r)=\sum_{m=0}^{\infty}p_m^4Q_m(r), \qquad (7)
$$

where $p_m^i(i=1,2,3)$ are the expansion coefficients and

$$
Q_m(r)=\sqrt{\frac{2m+1}{h_N-a}}P_m\left(\frac{2r-h_N-a}{h_N-a}\right) \qquad (8)
$$

with P_m being the mth Legendre polynomial. Theoretically, m runs from 0 to ∞. In practice, the summation over the polynomials in Eq. (7) can be halted at some finite value $m=M$ when higher-order terms become essentially negligible.

However, as is mentioned above, the conventional orthogonal polynomial method can only solve the multilayered curved plate when the material properties of two adjacent layers do not change significantly and cannot obtain correct continuous normal stress and normal electric displacement shapes. Here, we improve the orthogonal polynomial method so as to make it suitable for the multilayered piezoelectric spherical plates with or without very dissimilar material properties. We adopt, for each layer, specific shifted Legendre polynomials defined as follows:

- for the first layer: $$Q_m^1(r) = \sqrt{\frac{2m+1}{h_1-a}}\, P_m\left(\frac{2r-h_1-a}{h_1-a}\right) \tag{9.1}$$
- for the second layer: $$Q_m^2(r) = \sqrt{\frac{2m+1}{h_2-h_1}}\, P_m\left(\frac{2}{h_2-h_1}r - \frac{h_2+h_1}{h_2-h_1}\right) \tag{9.2}$$
- ...
- for the Nth layer: $$Q_m^N(r) = \sqrt{\frac{2m+1}{h_N-h_{N-1}}}\, P_m\left(\frac{2}{h_N-h_{N-1}}r - \frac{h_N+h_{N-1}}{h_N-h_{N-1}}\right) \tag{9.3}$$

Moreover, in order to automatically incorporate them into the calculation, the interface continuity conditions relative to the components of the mechanical displacement and to the electric potential, $u_a(a = 1, 2, 3)(u_r, u_\theta, u_z)$, and Φ are expanded as follows:

- In the first layer: $$\begin{cases} u_a^1 = \sum\limits_{m=0}^{\infty} p_{m,1}^a Q_m^1(r)\exp(ikb\varphi) \\ \Phi_1 = \sum\limits_{m=0}^{\infty} r_{m,1} Q_m^1(r)\exp(ikb\varphi) \end{cases}$$

  with: $$\begin{cases} u_a^1(r=h_1) = u_a^{1,h_1} = \sum\limits_{m=0}^{\infty} p_{m,1}^a Q_m^1(r=h_1)\exp(ikb\varphi) \\ \Phi_1(r=h_1) = \Phi_1^{h_1} = \sum\limits_{m=0}^{\infty} r_{m,1} Q_m^1(r=h_1)\exp(ikb\varphi) \end{cases} \tag{10.1}$$

- In the second layer: $$\begin{cases} u_a^2 = u_a^{1,h_1} + (r-h_1)\sum\limits_{m=0}^{\infty} p_{m,2}^a Q_m^2(r)\exp(ikb\varphi) \\ \Phi_2 = (r/h_1)^2\,\Phi_1^{h_1} + (r-h_1)\sum\limits_{m=0}^{\infty} r_{m,2} Q_m^2(r)\exp(ikb\varphi) \end{cases}$$

  with: $$\begin{cases} u_a^2(r=h_2) = u_a^{2,h_2} = u_a^{h_1} + (h_2-h_1)\sum\limits_{m=0}^{\infty} p_{m,2}^a Q_m^2(r=h_2)\exp(ikb\varphi) \\ \Phi_2(r=h_2) = \Phi_2^{h_2} = (h_2/h_1)^2\,\Phi_1^{h_1} + (h_2-h_1)\sum\limits_{m=0}^{\infty} r_{m,2} Q_m^2(r=h_2)\exp(ikb\varphi) \end{cases} \tag{10.2}$$

- In the third layer : $$\begin{cases} u_a^3 = u_a^{2,h_2} + (r-h_2)\sum\limits_{m=0}^{\infty} p_{m,3}^a Q_m^3(r)\exp(ikb\varphi) \\ \Phi_3 = (r/h_2)^2\,\Phi_2^{h_2} + (r-h_2)\sum\limits_{m=0}^{\infty} r_{m,3} Q_m^3(r)\exp(ikb\varphi) \end{cases}$$

  with: $$\begin{cases} u_a^3(r=h_3) = u_a^{3,h_3} = u_a^{2,h_2} + (h_3-h_2)\sum\limits_{m=0}^{\infty} p_{m,3}^a Q_m^3(r=h3)\exp(ikb\varphi) \\ \Phi_3(r=h_3) = \Phi_3^{h_3} = (h_3/h_2)^2\,\Phi_2^{h_2} + (h_3-h_2)\sum\limits_{m=0}^{\infty} r_{m,3} Q_m^3(r=h_3)\exp(ikb\varphi) \end{cases} \tag{10.3}$$

and so on ....

Substituting Eqs. (9) and (10) into Eq. (6), then multiplying by $Q_j^{1*}(r)$, $Q_j^{2*}(r)\ldots Q_j^{N*}(r)$, with j running from 0 to M, respectively, integrating over r from a to h_N, and taking advantage of the orthonormality of Legendre polynomials gives the following systems:

$$
\begin{aligned}
&{}^{n}A_{11}^{j,m}\,p_{m,n}^{1}+{}^{n}A_{12}^{j,m}\,p_{m,n}^{2}+{}^{n}A_{13}^{j,m}\,p_{m,n}^{3}+{}^{n}A_{14}^{j,m}\,p_{m,n}^{4}=-\omega^{2}\cdot{}^{n}M_{m}^{j}\,p_{m,n}^{1}, && (11.1)\\
&{}^{n}A_{21}^{j,m}\,p_{m,n}^{1}+{}^{n}A_{22}^{j,m}\,p_{m,n}^{2}+{}^{n}A_{23}^{j,m}\,p_{m,n}^{3}+{}^{n}A_{24}^{j,m}\,p_{m,n}^{4}=-\omega^{2}\cdot{}^{n}M_{m}^{j}\,p_{m,n}^{1}, && (11.2)\\
&{}^{n}A_{31}^{j,m}\,p_{m,n}^{1}+{}^{n}A_{32}^{j,m}\,p_{m,n}^{2}+{}^{n}A_{33}^{j,m}\,p_{m,n}^{3}+{}^{n}A_{34}^{j,m}\,p_{m,n}^{4}=-\omega^{2}\cdot{}^{n}M_{m}^{j}\,p_{m,n}^{1}, && (11.3)\\
&{}^{n}A_{41}^{j,m}\,p_{m,n}^{1}+{}^{n}A_{42}^{j,m}\,p_{m,n}^{2}+{}^{n}A_{43}^{j,m}\,p_{m,n}^{3}+{}^{n}A_{44}^{j,m}\,p_{m,n}^{4}=0 && (11.4)
\end{aligned}
$$

where ${}^{n}A_{\alpha\beta}^{j,m}(\alpha,\beta=1,2,3)$, and ${}^{n}M_{m}^{j}$ are the elements of a non-symmetric matrix. They can be obtained according to Eq. (6).

Equation (11.4) can be written as:

$$
p_{m,n}^{4}=-\left({}^{n}A_{44}^{j,m}\right)^{-1}\left({}^{n}A_{41}^{j,m}\,p_{m,n}^{1}+{}^{n}A_{42}^{j,m}\,p_{m,n}^{2}+{}^{n}A_{43}^{j,m}\,p_{m,n}^{3}\right). \tag{12}
$$

Substituting Eq. (12) into Eqs. (11.1), (11.2), and (11.3) gives:

$$
\begin{aligned}
&\left[{}^{n}A_{11}^{j,m}-{}^{n}A_{14}^{j,m}\left({}^{n}A_{44}^{j,m}\right)^{-1}\cdot{}^{n}A_{41}^{j,m}\right]p_{m,n}^{1}+\left[{}^{n}A_{12}^{j,m}-{}^{n}A_{14}^{j,m}\left(A_{44}^{j,m}\right)^{-1}\cdot{}^{n}A_{42}^{j,m}\right]p_{m,n}^{2}\\
&\quad+\left[{}^{n}A_{13}^{j,m}-{}^{n}A_{14}^{j,m}\left({}^{n}A_{44}^{j,m}\right)^{-1}\cdot{}^{n}A_{43}^{j,m}\right]p_{m,n}^{3}=-\omega^{2n}M_{m,n}^{j}\,p_{m,n}^{1}, && (13.1)\\
&\left[{}^{n}A_{21}^{j,m}-{}^{n}A_{24}^{j,m}\left({}^{n}A_{44}^{j,m}\right)^{-1}\cdot{}^{n}A_{41}^{j,m}\right]p_{m,n}^{1}+\left[{}^{n}A_{22}^{j,m}-{}^{n}A_{24}^{j,m}\left(A_{44}^{j,m}\right)^{-1}\cdot{}^{n}A_{42}^{j,m}\right]p_{m,n}^{2}\\
&\quad+\left[{}^{n}A_{23}^{j,m}-{}^{n}A_{24}^{j,m}\left({}^{n}A_{44}^{j,m}\right)^{-1}\cdot{}^{n}A_{43}^{j,m}\right]p_{m,n}^{3}=-\omega^{2n}M_{m,n}^{j}\,p_{m,n}^{1}, && (13.2)\\
&\left[{}^{n}A_{31}^{j,m}-{}^{n}A_{34}^{j,m}\left({}^{n}A_{44}^{j,m}\right)^{-1}\cdot{}^{n}A_{41}^{j,m}\right]p_{m,n}^{1}+\left[{}^{n}A_{32}^{j,m}-{}^{n}A_{34}^{j,m}\left(A_{44}^{j,m}\right)^{-1}\cdot{}^{n}A_{42}^{j,m}\right]p_{m,n}^{2}\\
&\quad+\left[{}^{n}A_{33}^{j,m}-{}^{n}A_{34}^{j,m}\left({}^{n}A_{44}^{j,m}\right)^{-1}\cdot{}^{n}A_{43}^{j,m}\right]p_{m,n}^{3}=-\omega^{2n}M_{m,n}^{j}\,p_{m,n}^{1}. && (13.3)
\end{aligned}
$$

Equation (13) can be written compactly as

$$
\begin{bmatrix}
{}^{n}\bar{A}_{11}^{j,m} & {}^{n}\bar{A}_{12}^{j,m} & {}^{n}\bar{A}_{13}^{j,m}\\
{}^{n}\bar{A}_{21}^{j,m} & {}^{n}\bar{A}_{22}^{j,m} & {}^{n}\bar{A}_{22}^{j,m}\\
{}^{n}\bar{A}_{31}^{j,m} & {}^{n}\bar{A}_{32}^{j,m} & {}^{n}\bar{A}_{33}^{j,m}
\end{bmatrix}
\begin{Bmatrix}
p_{m,n}^{1}\\ p_{m,n}^{2}\\ p_{m,n}^{3}
\end{Bmatrix}
=-\omega^{2}
\begin{bmatrix}
{}^{n}M_{m,n}^{j} & 0 & 0\\
0 & {}^{n}M_{m,n}^{j} & 0\\
0 & 0 & {}^{n}M_{m,n}^{j}
\end{bmatrix}
\begin{Bmatrix}
p_{m,n}^{1}\\ p_{m,n}^{2}\\ p_{m,n}^{3}
\end{Bmatrix}. \tag{14}
$$

So, Eq. (14) yields a form of the eigenvalue problem. The eigenvalue ω^2 gives the angular frequency of the guided wave; eigenvectors $p_{m,n}^{i}(i=1,2,3)$ allow the components of the particle displacement to be calculated; and $p_{m,n}^{4}$, which can be obtained thanks to Eq. (12), determines the electric potential distribution. According to $Vph=\omega/k$, the phase velocity can be obtained. The complex matrix Eq. (14) can be solved numerically making use of standard computer programs for the diagonalization of non-symmetric square matrices. $3N(M+1)$ eigenmodes are generated from the order M of the expansion and the layer number N. Acceptable solutions are those eigenmodes for which convergence is obtained as M is increased. We determine that the eigenvalues obtained are converged solutions when a further increase in the matrix dimension does not result in a significant change in the eigenvalues.

3 Numerical results

Based on the foregoing formulations, two computer programs have been written using Mathematica to calculate the dispersion curves and the field profiles for the multilayered piezoelectric spherical curved plates.

Table 1 Material parameters of the materials used in this section

Property	C_{22}	C_{23}	C_{12}	C_{33}	C_{13}	C_{11}	C_{55}	C_{66}	C_{44}
PZT-4	13.9	7.4	7.4	13.9	7.4	11.5	2.56	2.56	3.05
Hypothetical	139	74	74	139	74	115	256	256	305
BSN	23.9	10.4	5	24.7	5.2	13.5	6.5	6.6	7.6
	E_{26}	E_{35}	E_{12}	E_{13}	E_{11}	$\in_{22}$	$\in_{33}$	$\in_{11}$	ρ
PZT-4	12.7	12.7	−5.2	−5.2	15.1	650	650	560	7.5
Hypothetical	139.7	139.7	−57.2	−57.2	166.1	5,850	5,850	5,040	67.5
BSN	2.8	3.4	−0.4	−0.3	4.3	196	201	28	5.3

Units : $C_{ij}(10^{10}\mathrm{N/m^2})$, $\in_{ij}$ $(10^{-11}\mathrm{F/m})$, $e_{ij}(\mathrm{C/m^2})$, $\rho(10^3\mathrm{kg/m^3})$

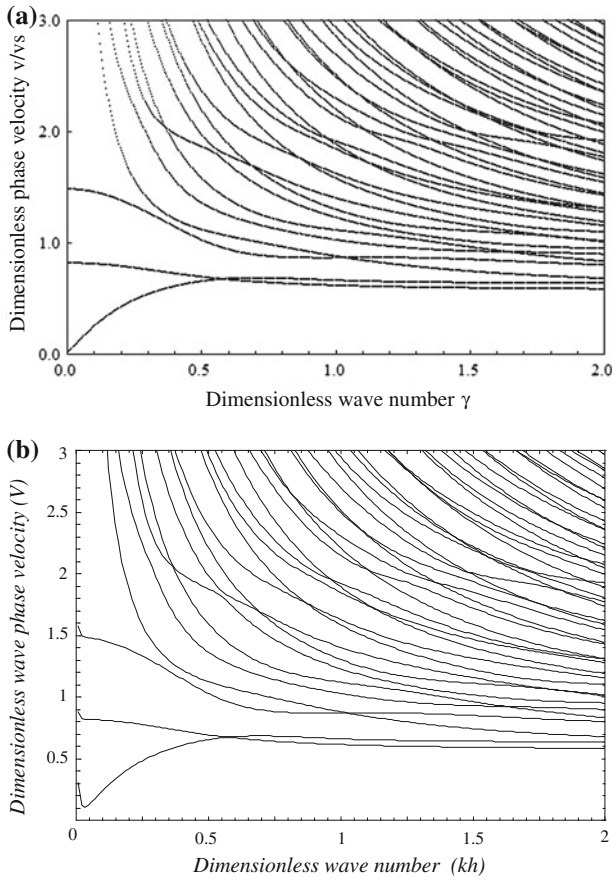

Fig. 2 Phase velocity dispersion curves for the two-layered piezoelectric structures; **a** the results from the reverberation-ray matrix method [6], **b** the results from the conventional polynomial method

3.1 Validation of the method in comparison with the exact solution obtained from the reverberation-ray matrix method

As is well known, the dispersion curves for a flat plate are the same as those for a spherical plate with a very large ratio of radius to thickness. So, we use the polynomial method to calculate a two-layered spherical plate with $\eta = 100$ to make a comparison with the corresponding flat plate. The spherical plate is composed of a BSN layer (inner layer) and a PZT-4 layer (outer layer) with equal thicknesses. Their material constants are shown in Table 1. Figure 2a shows the exact solution of the Lamb-like wave and SH-guided wave dispersion curves from the reverberation-ray method. Results are taken from Fig. 9 in [6]. It should be noted that Fig. 9 in *Science in China Series G* contains both the body wave modes and the Rayleigh wave modes. This paper just considers the guided waves (Lamb-like and SH-guided waves). Figure 2b is obtained from the conventional

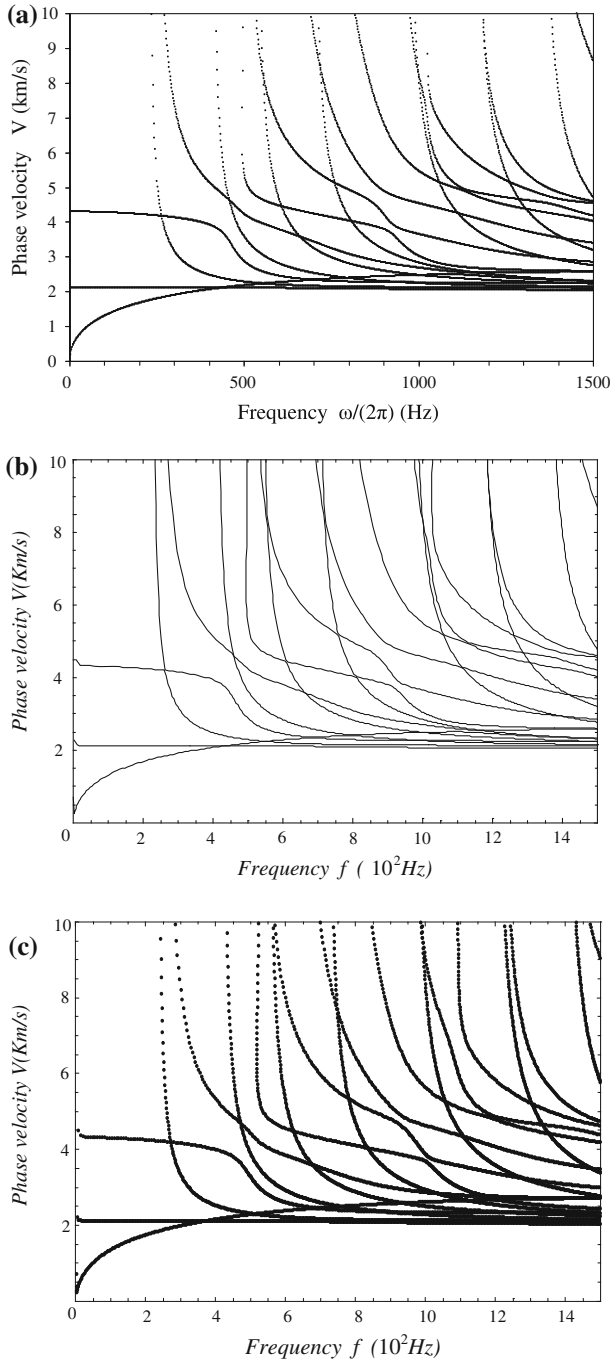

Fig. 3 Phase velocity dispersion curves for the three-layered piezoelectric structures with very dissimilar materials; **a** the results of the flat plate from the reverberation-ray matrix method, **b** the results of the spherical plate with $\eta = 100$ from the improved polynomial method, **c** the results of the spherical plate with $\eta = 100$ from the conventional polynomial method

polynomial approach. The solution of the improved polynomial approach is the same as in Fig. 2b. In order to save space, it is not shown here. As can be seen, Figs. 2a, b agree very well except at very small wave numbers (Wavelength at a very small wave number is very long, so that the influence of the curvature is considerable). So, we can say that for the two-layered piezoelectric structure without very dissimilar material parameters, the conventional polynomial approach can obtain correct dispersion curves.

Next, we show an example of a three-layered sandwich structure with very dissimilar materials, PZT-4/hypothetical material/PZT-4 with relative thicknesses 1/2/2. Here, in order to bring into play materials

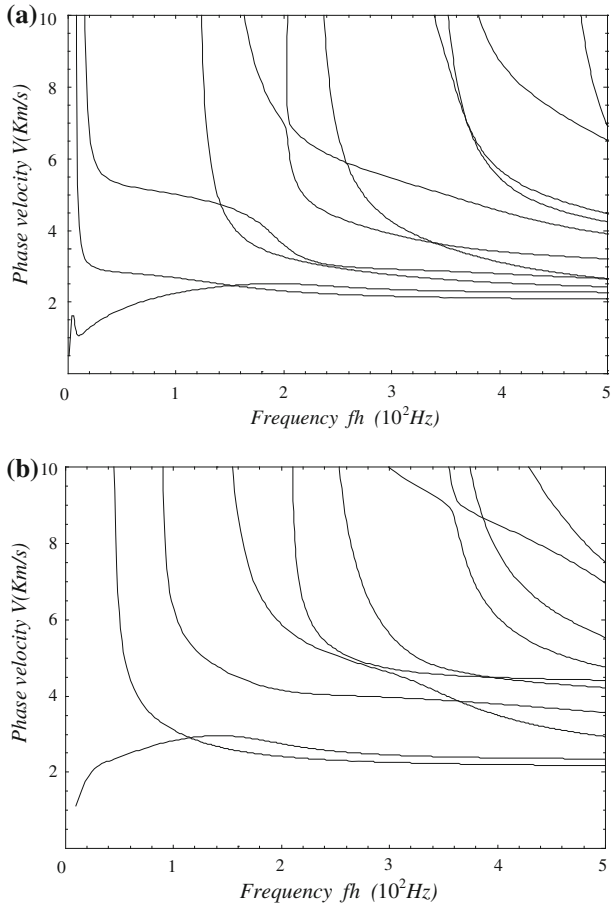

Fig. 4 Phase velocity dispersion curves for the P/B/P-1/2/2 layered piezoelectric spherical plate; **a** with $\eta = 10$, **b** with $\eta = 2$

with very dissimilar properties, a hypothetical material is used. Its material constants, about ten times higher than those of PZT-4, are also given in Table 1. Figure 3a shows the exact dispersion curves for the three-layered flat plate obtained from the reverberation-ray approach. Figures 3b, c give the dispersion curves for the three-layered spherical plate with $\eta = 100$ obtained from the improved and conventional polynomial approaches, respectively. It can be seen that Figs. 3a and b agree well. Figure 3c exhibits serious differences with Figs. 3a, b. This illuminates the validity of the improved polynomial approach.

3.2 Dispersion curves for the multilayered piezoelectric spherical plates

This section illustrates the influences of the radius-to-thickness ratio and of the stacking sequence on dispersion curves. The multilayered piezoelectric spherical plates are composed of BSN (B) and PZT-4 (P). Figure 4 shows the phase velocity dispersion curves for the P/B/P-1/2/2 multilayered piezoelectric spherical plate with (a) $\eta = 10$ and (b) $\eta = 2$. It illustrates the influence of the radius-to-thickness ratio. As the ratio decreases, the wave velocities and the cutoff frequencies increase. Figure 5 gives the phase velocity dispersion curves for the layered piezoelectric spherical plates with $\eta = 10$. The stacking sequence and thicknesses are (a) B/P/P-2/2/1 and (b) P/P/B-1/2/2. Comparing the three figures, Figs. 4a, 5a, b, we can see that although with the same material volume fractions and the same radius-to-thickness ratio, different stacking sequences result in very different dispersion curves.

3.3 Stress and electric displacement shapes

This section analyzes stress and electric displacement profiles for the Lamb-like waves of the above multilayered piezoelectric spherical plates. Figures 6 and 7 show stress and electric displacement profiles for the

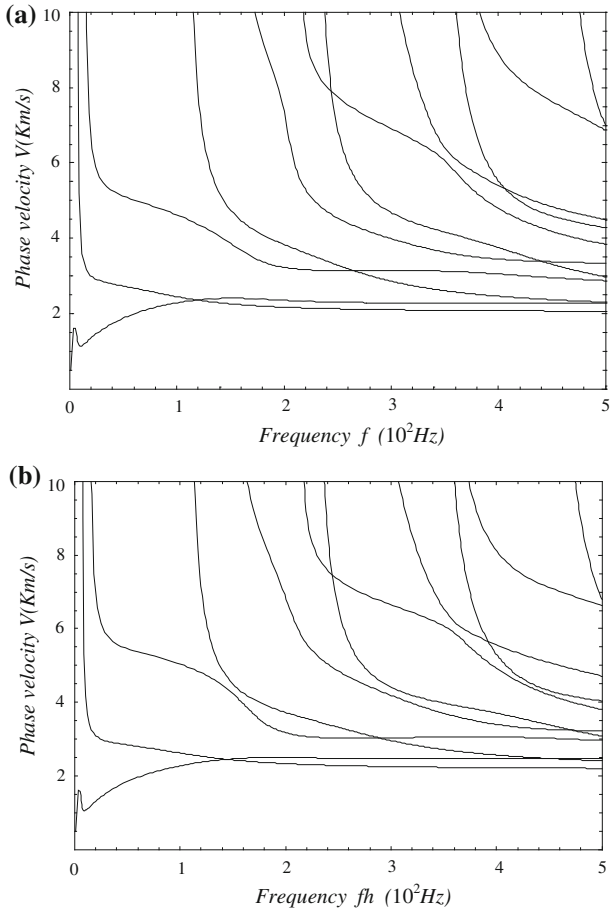

Fig. 5 Phase velocity dispersion curves for the three-layered piezoelectric spherical plates with $\eta = 10$; **a** B/P/P-2/2/1, **b** P/P/B-1/2/2

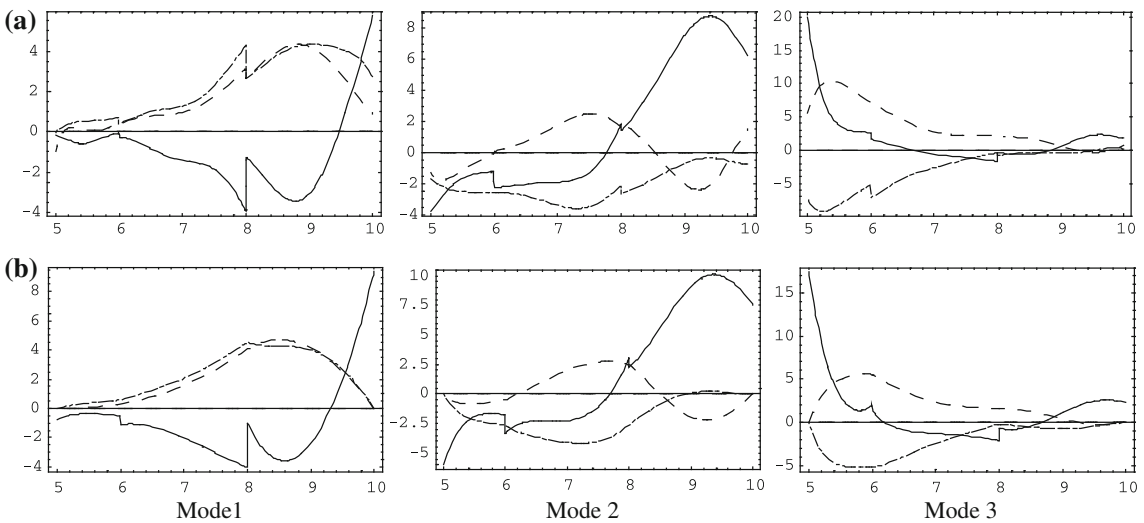

Fig. 6 Stress profiles for the P/B/P-1/2/2 spherical plate with $\eta = 2$ at $kh = 5.5$; *dashed line*: T_{rr}, *solid line*: $T_{\Phi\Phi}$, *Long-short-line*: $T_{r\Phi}$; *abscissa*: radial coordinate (unit: m), *ordinate*: stress (arbitrary units); **a** the conventional polynomial method, **b** the improved polynomial method

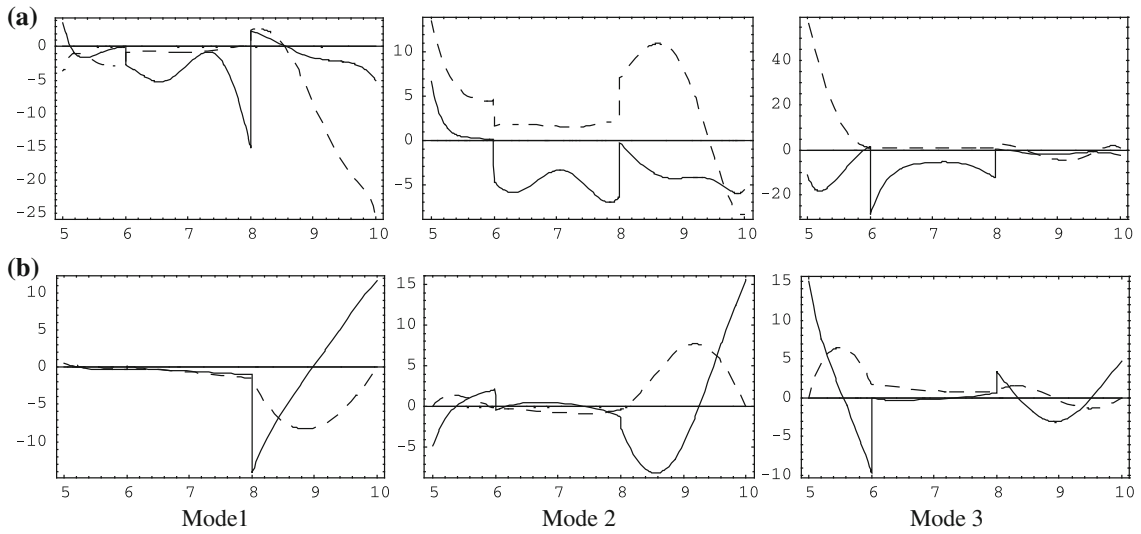

Fig. 7 Electric displacement profiles for the P/B/P-1/2/2 spherical plate with $\eta = 2$ at $kh = 5.5$; *dashed line*: D_r, *solid line*: D_Φ; *abscissa*: radial coordinate (unit: m), *ordinate*: electric displacement (arbitrary units); **a** the conventional polynomial method, **b** the improved polynomial method

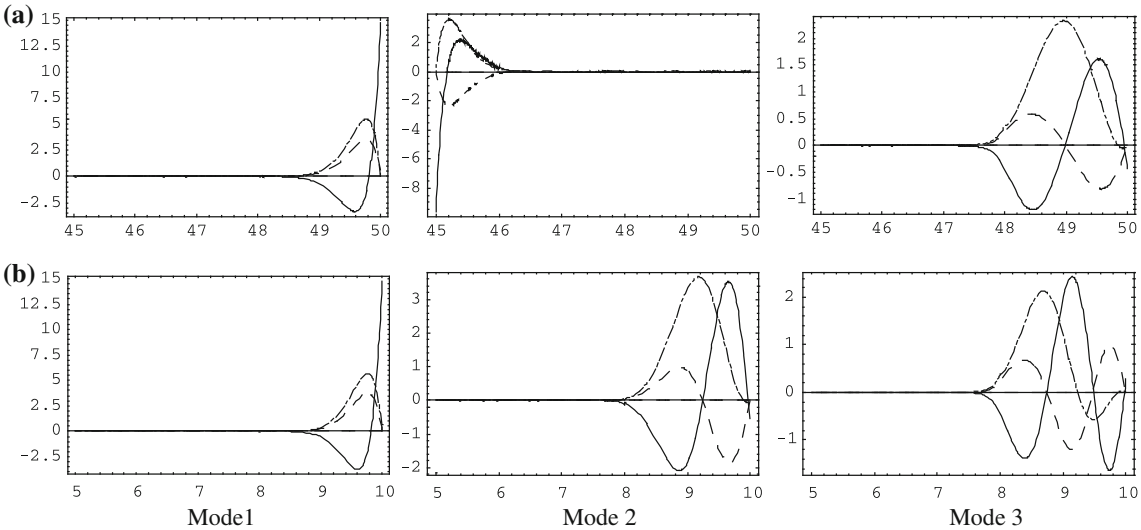

Fig. 8 Stress profiles for the P/B/P-1/2/2 spherical plate at $kh = 50.5$; *dashed line*: T_{rr}, *solid line*: $T_{\Phi\Phi}$, *Long-short-line*: $T_{r\Phi}$; *abscissa*: radial coordinate (unit: m), *ordinate*: stress (arbitrary units); **a** $\eta = 10$, **b** $\eta = 2$

P/B/P-1/2/2 spherical plate with $\eta = 2$ at $kh = 5.5$: Figs. 6a and 7a are obtained from the conventional polynomial method and Figs. 6b and 7b from the improved polynomial method. It can be seen that even for the layered spherical plate without dissimilar material properties, the conventional polynomial approach cannot give correct results. The obtained normal stress T_{rr}, $T_{r\varphi}$, and normal electric displacement D_r are discontinuous at the interfaces and they are not zero at the inner and outer surfaces, unlike the improved polynomial approach which overcomes these drawbacks. As expected, $T_{\varphi\varphi}$ and D_φ are not continuous at the interfaces and are not zero at the inner and outer surfaces. This also validates the improved method.

Figures 8 and 9 show the case of large wave number, $kh = 50.5$, for the P/B/P-1/2/2 spherical plates with $\eta = 10$ and 2, respectively. It can be seen that for the spherical plate with a large η, the stress and the electric displacement mainly distribute on the inner or outer layers. The inner or outer layers are all PZT-4. For the spherical plate with a small η, the stress and electric displacement just distribute on the outer layer PZT-4, but not on the inner layer PZT-4.

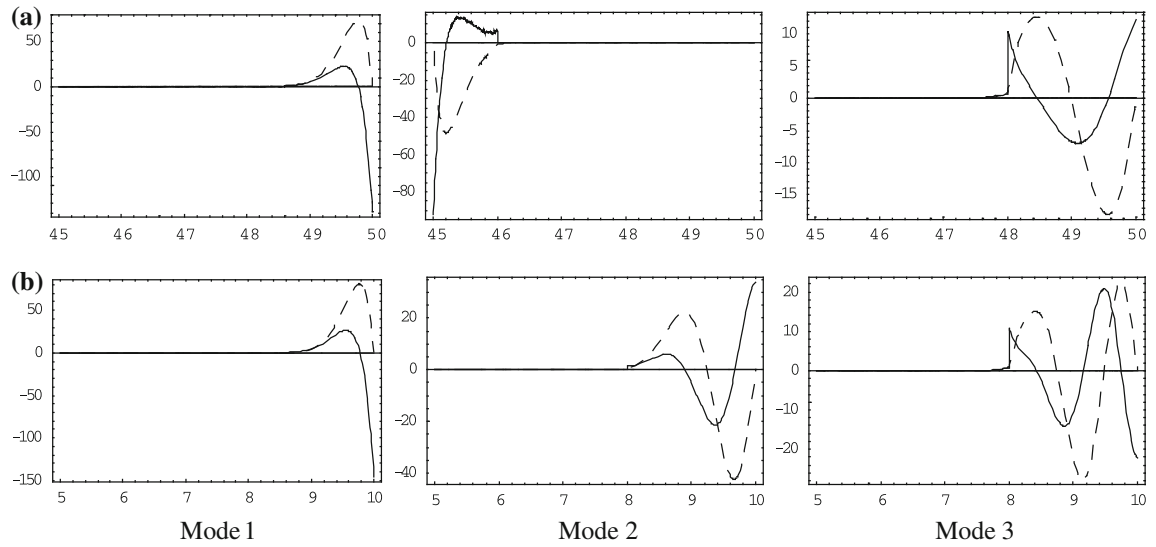

Fig. 9 Electric displacement profiles for the P/B/P-1/2/2 spherical plate at $kh = 50.5$; *dashed line*: D_r, *solid line*: D_Φ; *abscissa*: radial coordinate (unit: m), *ordinate*: electric displacement (arbitrary units); **a** $\eta = 10$, **b** $\eta = 2$

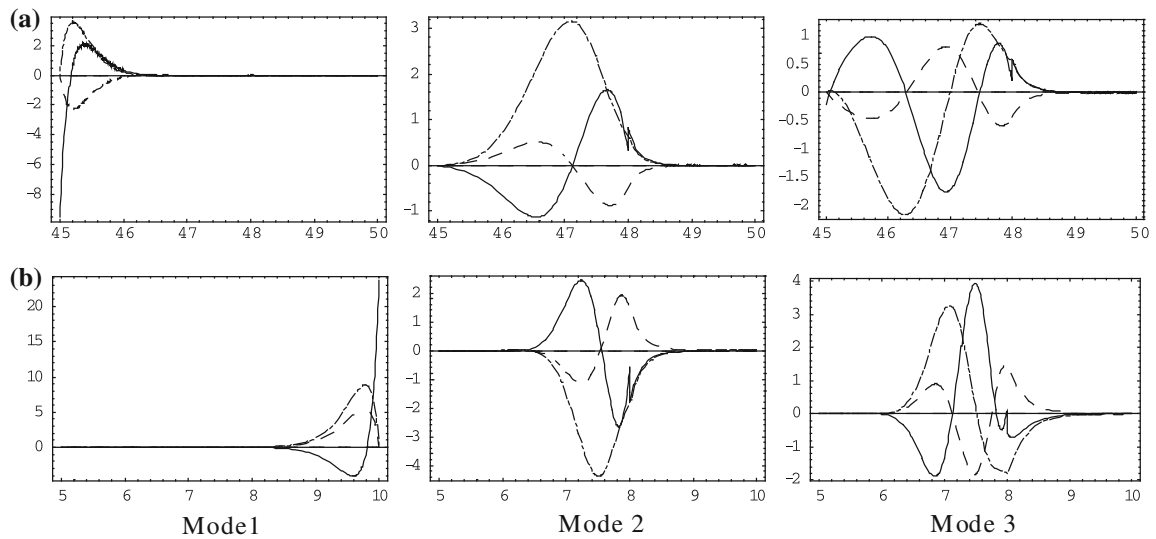

Fig. 10 Stress profiles for the P/P/B-1/2/2 spherical plate at $kh = 50.5$; *dashed line*: T_{rr}, *solid line*: $T_{\Phi\Phi}$, *Long-short-line*: $T_{r\Phi}$; *abscissa*: radial coordinate (unit: m), *ordinate*: stress (arbitrary units); **a** $\eta = 10$, **b** $\eta = 2$

Figures 10 and 11 give the cases of another stacking sequence, P/P/B-1/2/2 spherical plates with $\eta = 10$ and $\eta = 2$ at $kh = 30.5$. It can be seen that when the ratio η is large, the stress and the electric displacement always distribute on the inner and middle layers. The material of both layers is PZT-4. When the ratio η is small, the stress and electric displacement distribute on the outer layer BSN or middle layer PZT-4 (the outer side of the PZT-4 layer).

Making a comprehensive understanding about Figures 8, 9, 10, and 11, we can find two phenomena: (i) for a spherical plate with a large ratio η, the stress and electric displacement always distribute on the PZT-4 layer, whatever its position. The reason lies in that the wave speed of PZT-4 is lower than that of BSN. The high-frequency-guided waves always propagate in the layer with the lower wave speed. Simultaneously, the electric displacement also occurs in the layer with the lower wave speed. (ii) For a spherical plate with a small ratio η, besides the wave speed of the layer material, the position of the material is also important for the stress and electric displacement distributions. The distributions tend to move toward the outer layer for the spherical plate with a small ratio. As can be seen in Figs. 10b and 11b, the distributions of the first mode are on the

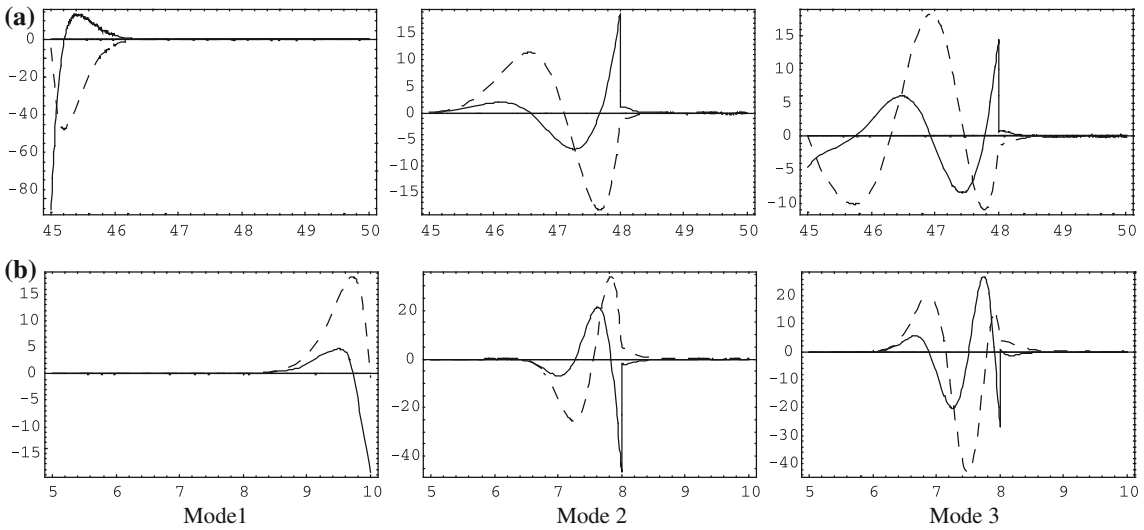

Fig. 11 Electric displacement profiles for the P/P/B-1/2/2 spherical plate at $kh = 50.5$; *dashed line*: D_r, *solid line*: D_Φ; *abscissa*: radial coordinate (unit: m), *ordinate*: electric displacement (arbitrary units); **a** $\eta = 10$, **b** $\eta = 2$

outer layer but not on the low-wave-speed layer. And the distributions of the second and third modes are on the middle layer (i.e., the outer layer PZT-4 but not the inner layer PZT-4).

4 Conclusions

Considering the intrinsic limitations of the orthogonal polynomial method, this paper proposed the improved orthogonal polynomial method to make it suitable for solving the multilayered piezoelectric spherical curved plate, whatever material properties. Through the numerical analysis, we can draw the following conclusions:

(a) Numerical comparison on dispersion curves and stress and electric displacement profiles verified that the improved method can correctly solve the wave propagation in a multilayered piezoelectric spherical plate whatever material properties.
(b) Radius to thickness ratio and stacking sequence have significant influences on dispersion curves and stress and electric displacement profiles.
(c) For a multilayered spherical plate with a large ratio η, stress and electric displacement of high frequency waves always distribute on the layer with the lower wave speed; for a spherical plate with a small ratio η, both wave speed and position of the layer are important for stress and electric displacement distributions.

Acknowledgments The authors appreciate the support by the National Natural Science Foundation of China (No. 11272115).

References

1. Goldberg, R.L., Jurgens, M.J., Mills, D.M et al.: Modeling of piezoelectric multilayer ceramics using finite element analysis. IEEE Trans. Ultrason. Ferroelectr. Freq. Control **44**, 1204–1214 (1997)
2. Ballandras, S., Reinhardt, A., Laude, V. et al.: Simulations of surface acoustic wave devices built on stratified media using a mixed finite element/boundary integral formulation. J. Appl. Phys. **96**, 7731–7741 (2004)
3. Nayfeh, A.H.: Wave Propagation in Layered Anisotropic Media with Applications to Composites. Elsevier, Amsterdam (1995)
4. Fahmy, A.H., Adler, E.L.: Propagation of acoustic surface wave in multilayers: a matrix description. Appl. Phys. Lett. **22**, 495–497 (1973)
5. Cai, C., Liu, G.R., Lam, K.Y.: A technique for modelling multiple piezoelectric layers. Smart Mater. Struct. **10**, 689–694 (2001)
6. Guo, Y.Q., Chen, W.Q., Zhang, Y.L.: Guided wave propagation in multilayered piezoelectric structures. Sci. China Ser. G: Phys. Mech. Astron. **52**, 1094–1104 (2009)
7. Xi, Z.C., Liu, G.R., Lam, K.Y., Shang, H.M.: Dispersion of waves in immersed laminated composite hollow cylinders. J. Sound Vib. **250**, 215–227 (2002)

8. Han, X., Liu, G.R., Ohyoshi, T.: Dispersion and characteristic surfaces of waves in hybrid multilayered piezoelectric circular cylinders. Comput. Mech. **33**, 334–344 (2004)
9. Pastureaud, T., Laude, V., Ballandras, S.: Stable scattering-matrix method for surface acoustic waves in piezoelectric multilayers. Appl. Phys. Lett. **80**, 2544–2546 (2002)
10. Kim, Y., Hunt, W.D.: Acoustic fields and velocities for surface-acoustic-wave propagation in multilayered structures: An extension of the Laguerre polynomial approach. JAP **68**, 4993–4997 (1990)
11. Lefebvre, J.E., Zhang, V., Gazalet, J., Gryba, T.: Legendre polynomial approach for modeling free ultrasonic waves in multilayered plates. JAP **85**, 3419–3427 (1999)
12. Datta, S., Hunsinger, B.J.: Analysis of surface waves using orthogonal functions. JAP **49**, 475–479 (1978)
13. Gubernatis, J.E., Maradudin, A.A.: A Laguerre series approach to the calculation of wave properties for surfaces of inhomogeneous elastic materials. Wave Motion **9**, 111–121 (1987)
14. Yu, J.G., Ma, Q.: Circumferential wave in functionally graded piezoelectric cylindrical curved plates. Acta Mech. **198**, 171–190 (2008)
15. Wu, B., Yu, J.G., He, C.F.: Wave propagation in non-homogeneous magneto-electro-elastic plates. J. Sound Vib. **317**, 250–264 (2008)
16. Elmaimouni, L., Lefebvre, J.E., Zhang, V., Gryba, T.: A polynomial approach to the analysis of guided waves in anisotropic cylinders of infinite length. Wave Motion **42**, 344–353 (2005)
17. Yu, J.G., Ding, J.C., Ma, Z.J.: On dispersion relations of waves in multilayered magneto-electro -elastic plates. Appl. Math. Model. doi:10.1016/j.apm.2012.01.028
18. Lefebvre, J.E., Zhang, V., Gazalet, J., Gryba, T., Sadaune, V.: Acoustic wave propagation in continuous functionally graded plates: An extension of the Legendre polynomial approach. IEEE Trans. Ultrason. Ferroelectr. Freq. Control **48**, 1332–1340 (2001)
19. Yu, J.G., Ratolojanahary, F.E., Lefebvre, J.E.: Guided waves in functionally graded viscoelastic plates. Compos. Struct. **93**, 2671–2677 (2011)
20. Elmaimouni, L., Lefebvre, J.E., Zhang, V., Gryba, T.: Guided waves in radially graded cylinders: a polynomial approach. NDT&E Int. **38**, 344–353 (2005)
21. Yu, J.G., Xue, T.L.: Generalized thermoelastic waves in spherical curved plates without energy dissipation. Acta Mechanica **212**, 39–50 (2010)
22. Yu, J.G., Wu, B.: Circumferential wave in magneto-electro-elastic functionally graded cylindrical curved plates. Eur. J. Mech. A/Solids **28**, 560–568 (2009)
23. Yu, J.G., Wu, B., He, C.F.: Guided thermoelastic waves in functionally graded plates with two relaxation times. Int. J. Eng. Sci. **48**, 1709–1720 (2010)
24. Yu, J.G., Ma, Q., Su, S.: Wave propagation in non-homogeneous magneto-electro-elasitc hollow cylinders. Ultrasonics **48**, 664–677 (2008)
25. Yu, J.G., Ma, Q.: Wave characteristics in magneto-electro-elastic functionally graded spherical curved plates. Mech. Adv. Mater. Struct. **17**, 287–301 (2010)
26. Yu, J.G., Ma, Z.J.: Guided viscoelastic wave in circumferential direction of orthotropic cylindrical curved plates. Struct. Eng. Mech. **41**, 605–616 (2012)
27. Kargl, S.G., Marston, P.L.: Ray synthesis of Lamb wave contributions to the total scattering cross section for an elastic spherical shell. J. Acoust. Soc. Am. **88**, 1103–1113 (1990)
28. Towfighi, S., Kundu, T.: Elastic wave propagation in anisotropic spherical curved plates. Int. J. Solids Struct. **40**, 5495–5510 (2003)